Translational energy and state resolved observations of D and D$_2$ thermally desorbing from D clusters chemisorbed on graphite

S. Baouche,[1,2] L. Hornekær,[2] A. Baurichter,[1] A. C. Luntz,[1,2,a)] V. V. Petrunin,[1] and Ž. Šljivančanin[2,3]

[1]*Institute of Physics and Chemistry, University of Southern Denmark, Odense DK-5230, Denmark*
[2]*Institute of Physics and Astronomy, University of Aarhus, Aarhus DK-8000, Denmark*
[3]*Vinča Institute of Nuclear Sciences (020), P.O. Box 522, Belgrade RS-11001, Serbia*

Direct D atom desorption, as well as associative desorption of D$_2$ molecules are observed in thermal desorption from D atoms chemisorbed on a C(0001) surface by combining laser induced T-jumps with resonance enhanced multiphoton ionization detection. Bleaching curves suggest that different classes of chemisorbed D atom clusters are present on the initial surface. The energy resolved atomic desorption flux, obtained via time of flight techniques, compares favorably (via detailed balance) with theoretical calculations of atomic sticking. Density functional theory calculations of chemical processes (atomic desorption, atomic diffusion/cluster annealing, and associative desorption) on an extensive set of four atom H(D) clusters chemisorbed on C(0001) provide a good interpretation of the experiments. State and energy resolved D$_2$ desorption fluxes are compared with previous state averaged results. In combination with density functional theory calculations these measurements reveal a substantial energy loss (>1 eV) to the surface in the associative desorption. © *2009 American Institute of Physics.* [doi:10.1063/1.3274655]

I. INTRODUCTION

There has been much interest and activity over the past decade in the interaction of hydrogen atoms and molecules with graphite and other chemically similar forms of carbon (SWNT, graphene, etc.). Much of this interest is stimulated by the possibility of using one or the other forms of C as a hydrogen storage material and for its role in the formation of molecular H$_2$ in the interstellar medium. The latter process is generally believed to occur via recombination of H atoms on dust grains[1] that are principally either silicates or graphite-like, e.g., graphite onionlike particles or polycyclic aromatic hydrocarbons.[2]

It was originally suggested in electronic structure calculations,[3,4] and subsequently confirmed experimentally,[5] that H atoms incident from the gas phase can weakly chemisorb over an atop site on the C(0001) terrace by breaking some of the π bonding and puckering the atop C out of the plane. From density functional theory (DFT) calculations, the binding energy of a single H atom to the basal plane of C(0001) is ~ 0.7 eV, with a C atom puckering of ~ 0.4 Å and with a barrier to entrance into the chemisorption well of ~ 0.2 eV from gas phase H+C(0001).[4] Scanning tunneling microscopy (STM) experiments[6,7] and DFT calculations[6] show that at low H coverage Θ_H, the H is preferentially adsorbed as dimers rather than as random monomers, and that these dimers account for the puzzling first order H$_2$ associative desorption kinetics that was observed when thermally annealing the surface.[5] The para- and ortho-oriented dimers are the most stable configurations and the preferred recombination path to H$_2$ is via the paradimer.[6] Diffusion

barriers from the ortho- to para configuration are slightly higher than the para recombination barrier, and this accounts for a second slightly higher peak in the temperature programmed desorption (TPD) of H$_2$ from C(0001).[6] The DFT calculations also indicate that H diffusion barriers are moderately large (>1 eV), but that the barrier to H adsorption into the dimer configurations relative to the monomer adsorption is <0.2 eV or even nonexistent.[8] Thus, the latter is the predominate reason for formation of dimers at low Θ_H.

At higher Θ_H, STM experiments see larger and more complex clusters as well as dimers.[8,7] In the limit of saturation coverage, $\Theta_H \sim 0.4$,[5,9] atomic resolution is entirely lost so that the underlying C lattice is not even visible.[8,7] DFT calculations[8,10] demonstrate that barriers to H adsorption are small or negligible for some configurations of the larger clusters, as well as for formation of the dimer, and therefore larger clusters are readily produced via increased H exposure. The calculations[10] show that the average H binding energy increases with cluster size and this provides a thermodynamic driving force for the formation of large clusters at higher Θ_H. However, they also show that for a given cluster size, there is great variability in the stability of the different cluster configurations. The lowest barriers to associative desorption of H$_2$ from the larger clusters are via local para-configurations in the clusters and are similar in magnitude with those of the dimers. Therefore, the TPD peak for associate desorption of H$_2$ at higher Θ_H is similar to that at low Θ_H (except for relative intensities).

We previously measured the internal state averaged translational energy distribution of H$_2$ (D$_2$) associatively desorbing from a H(D) saturated C(0001) surface.[11] These experiments measured the time of flight (TOF) for the associa-

tively desorbed H_2 (D_2) induced by a pulsed IR laser T-jump of the surface. Broad translational energy distributions normal to the surface were observed, peaking at ~1.3 eV and extending to ~3.4 eV, the energetic limit calculated via DFT for associative desorption from the para dimer configuration. It was not, however, possible to determine whether the modest average translational energy observed (relative to that available) and the large breadth of the distribution were caused by populating many internal states in the associative desorption, a broad lower distribution in available desorption energies due to variations in barriers to associative desorption (relative to the dimer), or a large and broad distribution in energy loss to the surface in the desorption process. The angular distribution for the associative desorption was highly peaked normal to the surface and no isotope effect was observed.

To date, no atomic H or D desorption from C(0001) has been directly observed. Only associative H_2 (D_2) desorption is observed in TPD experiments at all Θ_H (Θ_D). Of course, the experimental configuration used in TPD experiments (measuring background chamber pressure) precludes the direct observation of atomic desorption. Indirect isotope scrambling experiments suggest that some atomic desorption may also occur.[12] The residence time of the monomer on the surface is estimated from DFT calculations[8] to be only ~6 min due to atomic desorption at T_s ~ 300 K, and significantly less at higher T_s. Certainly at T_s ~ 200 K, STM observes that some monomer H is also produced at low Θ_H but that it disappears in thermal annealing.[8] There is, however, no direct evidence for atomic desorption at higher Θ_H (Θ_D) from the larger clusters. Atomic desorption is of great interest since state of the art "first principles" calculations of the time reversed process of atomic adsorption have recently been reported,[13,14] and the atomic desorption should be related to the atomic adsorption through detailed balance.

In this paper, we report direct measurements of atomic D and molecular D_2 desorbed from C(0001) as the result of a laser induced T-jump of the C(0001) surface to temperature T_p at various initial chemisorbed Θ_D, and especially at saturation coverage. These experiments measure the desorption of both species induced by the T-jump via (2+1) resonantly enhanced multiphoton ionization (REMPI) using a tunable pulsed UV laser. The TOF distributions of the desorbing atoms and molecules are measured by varying the time delay between the REMPI laser and the T-jump laser, and this determines the energy distribution of the desorbing flux $D_f(E,T_p)$ of each species. Using detailed balance, the atomic adsorption $S(E,T_p)$ is obtained from $D_f(E,T_p)$ for D atoms and compared with the theoretical adsorption calculations mentioned above.

II. EXPERIMENTAL

All experiments are carried out in a stainless steel ultra-high vacuum (UHV) chamber with a base pressure of ~10^{-10} torr that has been described in detail previously.[11] Briefly, the chamber contains a resistively heated tungsten tube atom source for generation of thermal H (D) atoms (MBE-components), a differentially pumped quadrupole mass spectrometer for measuring TPD from the surface, a differentially pumped rotatable quadrupole mass spectrometer for measuring the TOF of laser desorbed molecules and a TOF ion detector to measure laser desorbed atoms and molecules via REMPI. A ZYA grade highly ordered pyrolytic graphite (HOPG) sample is glued to a tantalum disk that can be heated by electron bombardment on its back face. Combined with water cooling, the HOPG temperature range is 290–1400 K as measured by a C-type thermocouple placed between the HOPG back face and the tantalum disk. Before introduction into the UHV chamber, the HOPG sample is repeatedly peeled using adhesive tape until a visually flat surface is obtained. Following bake out, the sample is annealed to 1350 K for several minutes so that a clean surface is obtained with minimal defects. The sample surface quality is repeatedly monitored via TPD from the HOPG of H_2 (D_2) and hydrocarbon fragments at saturation Θ_H (Θ_D) as these are sensitive to the presence of defects such as step edges.[15]

The H (D) source generates atomic beams with thermal energies between 1800 and 2200 K and H(D) fluxes from 10^{-3} to 2×10^{-2} ML s^{-1}, (1 ML=3.8×10^{15} cm^{-2}) depending on the H_2 (D_2) pressure in the tube of the doser. The background pressure in the UHV chamber is typically P =1.5×10^{-8} torr during dosing. For most of the experiments reported here, the source temperature is 2200 K. The HOPG surface is 18 cm from the directed doser and is exposed for a specified amount of time to create a H or D coverage Θ_H (Θ_D). The saturation coverage is Θ_H (Θ_D) $\approx$ 0.4.[9] A fresh dose of D or H atoms is used for each REMPI experiment. No measurable isotope effect is observed in either the atomic or molecular desorptions. Therefore, we only present results for D and D_2 desorption because this isotope gives somewhat better signal/noise in experiments due to lower backgrounds and better energy resolution in the ion TOF.

A pulsed Nd:YAG-laser at 1064 nm incident on the surface at ~45° from the surface normal creates a T-jump at the surface and induces all adsorbate chemistry: D desorption, D_2 associative desorption, and diffusion/annealing of the surface. The output of the IR laser is apertured in the near field region of the laser and this aperture is optically imaged onto the surface thereby creating a nearly top hat (approximately constant laser intensity) spot on the surface of ~2.3 mm^2 area. The 10 Hz laser has a 16.5 ns pulse width. The T-jump of the HOPG surface induced by the laser irradiation is calculated by solving the coupled differential equations describing the time resolved heat formation and propagation via a three dimensional spatial finite element and time resolved model.[16] This modeling shows that the surface temperature reaches its peak with a small delay relative to the laser pulse of ~12 ns and that its duration is ~50 ns. The optical absorption depth is only ~40 nm, so only the near surface region is appreciably heated. The magnitude of the peak surface temperature in the T-jump T_p depends on laser intensity and is thus readily controlled during the experiments. T_p is given by the model as $T_p \approx 290$ K+$7.4F_\omega$, where F_ω is the laser fluence in mJ/cm^2. The first term describes the rest temperature of the surface and the second the laser induced T-jump. The only significant uncertainty in this model is the value of the thermal conductivity between graphite planes,
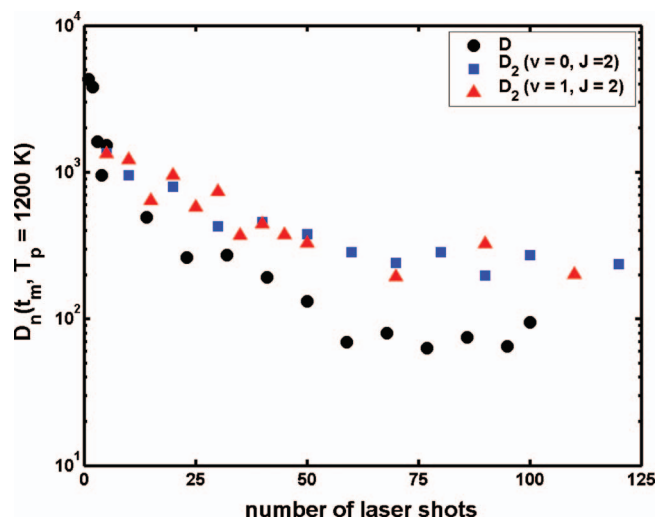
FIG. 1. D and D$_2$ state resolved bleaching of the desorption density $D_n(t_m, T_p = 1200 \text{ K})$ from $\Theta_D \approx 0.4$ chemisorbed on C(0001) induced by laser T-jumps to a peak temperature of $T_p \sim 1200$ K. All desorbed species are measured by the REMPI intensity at the peak of the time of the flight distribution t_m and as a function of the number of prior laser shots. Desorbed species/internal states are as identified in the legend.

which appears to be sample dependent since there is some variability in the literature. This confers an uncertainty in T_p of ~ 200 K (at high laser fluence). Indirect experimental measurements of T_p via the temperature of the Maxwell–Boltzmann velocity distribution describing hydrocarbon fragments desorbed from a defected surface are in good agreement with this model.[16] However, it should be emphasized that none of the details of the processes described in this paper depend on an accurate knowledge of T_p. Typically, laser fluences $F_\omega < 150$ mJ/cm^2 were utilized for the T-jumps and at this fluence there was no irreversible defect formation at the surface as monitored by subsequent TPD of adsorbed H. At higher fluences, however, TPD of adsorbed H did indicate some surface defect formation. These defects were easily removed by a slow anneal to 1350 K.

The chemistry induced by this T-jump is similar to the conventional thermally induced chemistry observed in TPD, but with an ultrafast temperature ramp of $10^{10} - 10^{12}$ K/s. All chemical processes, i.e., diffusion, atomic desorption, and associative desorption, are described in terms of simple first order thermal kinetics, with rate constants given by $k_i = v_i \exp(-V_i / k_B T)$, where $i = d, a, m$ for diffusion, atomic desorption, and molecular associative desorption, respectively. v_i is the pre-exponential for the rate and V_i is the barrier for the process. Because the temperature dependences for all processes are dominated by the exponential terms, most of the chemistry occurs at or near the peak temperature, and when yields for the chemistry per laser pulse are small, the chemistry is well approximated as an isothermal processes at T_p.[17] Repeated laser shots at a given surface spot ultimately bleach the signal due to inducing D$_2$ (and D) desorption. By monitoring the bleaching curve, the number of desorbed molecules per laser shot is estimated. For the laser intensities used in the experiments reported here, desorption yields are quite small, typically <0.02 ML/pulse (see Fig. 1). After bleaching one laser spot area, the sample is moved parallel to

its surface to expose another irradiation area that does not overlap with the previous one. Seven different spots are irradiated on the HOPG in this way and desorption results averaged. In addition, TOF results represent averages over several independent D exposures on the surface because of the low signal to noise in these experiments.

2+1 REMPI of D and D$_2$ detect the atomic and molecular components, respectively, in the desorption flux generated via the T-jump of C(0001) surfaces with Θ_D coverage. In contrast with the majority of previously reported REMPI experiments utilizing the $S_{1/2}$-$2S_{1/2}$ atomic two-photon transition,[18] we use the slightly weaker $1S_{1/2}$-$3S_{1/2}$ two-photon resonance (ca. 205 nm) as the resonant two-photon step in the REMPI of the atoms. This choice allows us to switch the REMPI detection scheme between atoms and molecules without change of the laser dye and any serious modifications in the nonlinear frequency doubling and mixing sections of the laser system. State resolved detection of desorbed D$_2$(v,J) is also observed using (2+1) REMPI transitions via the $(X\,^1\Sigma_g^+ \rightarrow E, F\,^1\Sigma_g^+)$ electronic band as the resonant two-photon step.[19] We use the $\Delta v = 0$, $\Delta J = 0$ transitions in $(X\,^1\Sigma_g^+ \rightarrow E, F\,^1\Sigma_g^+)$ so that all rotational states with $J < 15$ for both vibrational states can be detected without major changes in the laser system. Most molecular experiments reported here measured the v=0, J=2 and v=1, J=2 states of D$_2$. Only D$_2$ was probed via REMPI since there is a significant background of H$_2$ in the UHV chamber. We have, however, shown previously that there is no measurable isotope effect in the internal state averaged associative desorption.[11]

The UV laser used for the REMPI (202–210 nm) is produced by frequency tripling a commercial Nd:YAG pumped dye laser in the range 606–630 nm (Continuum ND6000). The resulting UV is ~ 5 ns duration pulses with 0.35–0.5 mJ fluence and with 0.1–0.2 cm^{-1} spectral width. The UV laser beam is focused inside the UHV chamber to a ~ 0.1 mm diameter beam waist parallel to the sample surface and positioned at distance l from the surface. The UV laser is aligned to the center of the T-jump laser spot on the surface by translating it parallel to the surface while monitoring the REMPI intensity from D or D$_2$ desorbed by the T-jump. The distance between the UV laser focus and the sample surface l is set by accurately translating the UV laser beam normal to the surface from the point where it strikes the surface. Overall alignment uncertainty in l is estimated as 0.1 mm. Most experiments use $l = 2.9$ mm. In the T-jump, desorption occurs over a time that is much smaller than the flight time of atoms or molecules to the focus of the UV laser. The two pulsed lasers are synchronized by external trigger electronics and TOF techniques can be used to measure the translational energy distributions of the desorbing species by measuring the REMPI intensity as a function of the delay between the REMPI laser and the T-jump laser. The REMPI intensity for the various desorbed species is measured by the ion signal on a microsphere channel plate at the end of a TOF tube, where the flight time selects the appropriate mass of the ionized species. Data acquisition is with a digital storage oscilloscope (LeCroy WaveSurfer 452 500 MHz 2 GS/s) which allows detection of the REMPI intensity for each laser

T-jump and REMPI laser pair. Postaveraging in any appropriate manner is done subsequently in a computer. The principal uncertainty in the TOF (and hence in the energy resolution) is uncertainty in l which limits the TOF to $\sim 3\%$ accuracy and energy resolution to $\sim 6\%$.

The REMPI intensity I_i for either the atoms or molecules desorbed in the T-jump is proportional to the ith state-resolved desorption density $D_n(i,t)$, i.e., $I_i(t) \propto D_n(i,t)I_{uv}^2$, where I_{uv} is the UV laser intensity. It is assumed that the last photoionization step is fully saturated because of the high laser spectral density and tight laser focus.[19] With the laser wavelength selected to probe either atoms or a fixed v, J state of D_2, translational energy distributions normal to the surface (E) are obtained by measuring the TOF from the surface to the focused UV laser beam by varying the delay t between the pulsed UV laser and the IR pulsed laser inducing the T-jump and desorption. The small time lag between the desorption peak and the T-jump laser (ca. 12 ns) is minimal compared to typical flight times of ~ 600 ns. Desorption fluxes at surface temperature T_p are obtained from the TOF signals in the usual manner via Eq. (1), where m_i is the mass of the i desorbing species,

$$D_f(i,E,T_p) = t^2 D_n(i,t,T_p) \quad \text{and} \quad E = \frac{1}{2} m_i \left(\frac{l}{t}\right)^2. \quad (1)$$

Using detailed balance, the desorption flux can be converted to the time reversed process of sticking $S(i,E,T_p)$ for comparison with theoretical calculations via Eq. (2).

$$D_f(i,E,T_p) \propto E \exp(-E/k_B T_p)\exp(-\varepsilon_i/k_B T_p)S(i,E,T_p), \quad (2)$$

where ε_i is the internal energy of the ith state. For atom desorption, $\varepsilon_i = 0$.

No attempt was made to accurately compare relative $D_n(i,t)$ for the various i species; D atoms, $D_2(v=0)$ and $D_2(v=1)$ because the wavelength changes necessary to detect the various species caused significant optical realignment of the REMPI excitation system. We note, however, that REMPI intensities for $D_2(v=0) > D_2(v=1) \gg D$. The D atom desorption flux is estimated by comparing the REMPI intensity from laser induced desorption to that of the D atom beam source used in the dosing since this density is roughly known. The total D_2 and D desorption flux integrated over the bleaching is known from the coverage. This indicates that associative desorption is the dominate desorption mechanism.

III. EXPERIMENTAL RESULTS

Both D and D_2 are observed by 2+1 REMPI following a laser induced T-jump to ~ 1200 K of the HOPG with Θ_D at saturation. Both v=0, J and v=1, J D_2 are easily observed. All species show characteristic TOF distributions (as described later) and the density of desorbed D and D_2 are taken to be proportional to the REMPI intensity of the respective peaks of the TOF distributions t_m since the TOF distributions are nearly independent of F_ω. As shown in Fig. 1, the desorption of both species bleaches with repeated laser shots due to desorption of D_2 and D from the irradiated spot and

the lowering of Θ_D in the chemisorbed state for subsequent laser shots and due to thermal annealing of the chemisorbed state. The D desorption show a rapid initial bleaching, followed by a slower bleaching at the same rate as that for the molecules. The atomic bleaching rate is approximately represented as the sum of two exponentials, loosely defining an initial rate of bleaching R_i and a later rate of bleaching which is also characteristic for the molecular bleaching and therefore labeled R_m. Previous experiments measuring internal state averaged D_2 associative desorption induced by a laser T-jump also showed bleaching and demonstrated that diffusion into the bleached spot from adjoining areas did not occur during the sequence of laser shots.[11] Figure 1 suggests that atoms from two types of clusters are desorbed during the sequence of laser shots. Since the initial desorption must represent the most weakly bound D, desorption characterized by R_i is identified as D desorption from less stable cluster configurations with weakly bound D, while the desorption characterized by R_m originates from more stable cluster configurations with more strongly bound D.

Thermally annealing a freshly prepared surface with Θ_D at saturation to 510 K for 1 min prior to laser induced desorption exhibits only the slow bleaching curve characterized by R_m and with roughly the same intensity as for the sample that has been subjected only to the prior laser shots. This suggests that several prior laser T-jumps is equivalent to a slow thermal anneal. Presumably, the thermal or laser T-jump anneal desorbs D from less stable D sites and simultaneously converts the D clusters to the most stable configurations via D atom diffusion, as well as inducing simultaneous D_2 associative desorption. Note that this interpretation also implies that D_2 associative desorption occurs principally from para dimer configurations in the most stable larger clusters, just as for the dimers.[6] From the approximate estimates of the various detected desorption fluxes discussed earlier, we estimate that the atomic desorption integrated over the laser induced bleaching accounts for $\sim 5\%$ of the total desorption. This estimate is used to scale the D to D_2 desorption intensities in Fig. 1 and implies that initial desorption from the metastable large clusters is dominated by atomic desorption, but that after some thermal annealing to the more stable cluster configurations, molecular associative desorption dominates the desorption process.

Figure 2 shows bleaching curves for D desorption for a T-jump to $T_p \sim 1500$ K for different initial Θ_D as indicated in the figure. Θ_D is estimated in this figure by assuming a saturation coverage of 0.4 for ~ 8 ML D exposure and using relative TPD intensities of D_2 associative desorption to scale Θ_D for lower D exposures. This figure shows (1) that the flux of D desorption for the first few laser shots is nearly independent of Θ_D while it is proportional to Θ_D for the later shots, (2) that R_i decreases with Θ_D, and (3) that R_m is nearly independent of Θ_D. Following the interpretation suggested for Fig. 1, this implies that upon initial exposure to the D atom beam (low Θ_D), principally small cluster configurations are produced (due to limited D diffusion) with many low stability D sites. As Θ_D increases and the cluster size grows,
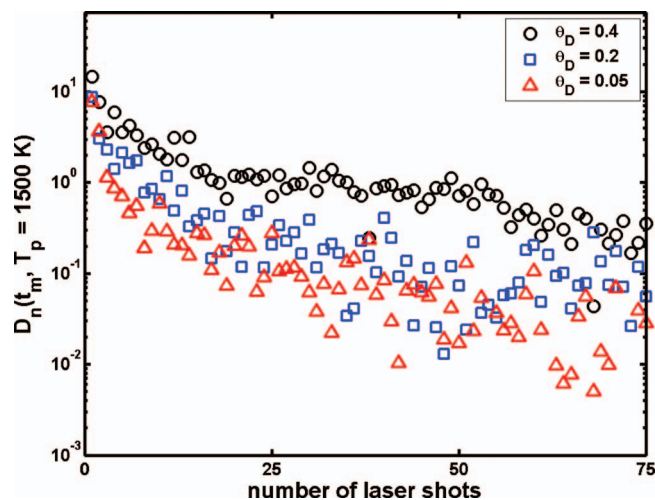
FIG. 2. D atom bleaching of the desorption density $D_n(t_m, T_p = 1500$ K) at different Θ_D chemisorbed on C(0001) induced by laser T-jumps to a peak temperature of $T_p \sim 1500$ K. Desorbed atom density is measured by the REMPI intensity at the peak of the time of the flight distribution t_m as a function of the number of prior laser shots.

both the number of unstable and stable D sites (perhaps produced principally via thermal annealing of less stable sites via prior laser shots) in the clusters increase.

As described previously, the TOF density distribution of atoms and molecules desorbed from the surface are obtained by varying the delay between the REMPI laser and the T-jump laser. This is converted to $D_f(i, E, T_s)$ via Eq. (1) and subsequently to $S(i, E, T_s)$ via Eq. (2). Because the flight distance from the surface to the REMPI laser ionization volume is small (typically ~2.9 mm), it is important to ensure that it is determined accurately (to ~0.1 mm) to give an accurate transformation between t and E in Eq. (1). Figure 3 shows $D_f(i, E, T_s)$ for v=0, J=2 and v=1, J=2 D$_2$ from associative desorption from REMPI following a T-jump to T_p ~1400 K compared to that obtained previously via laser
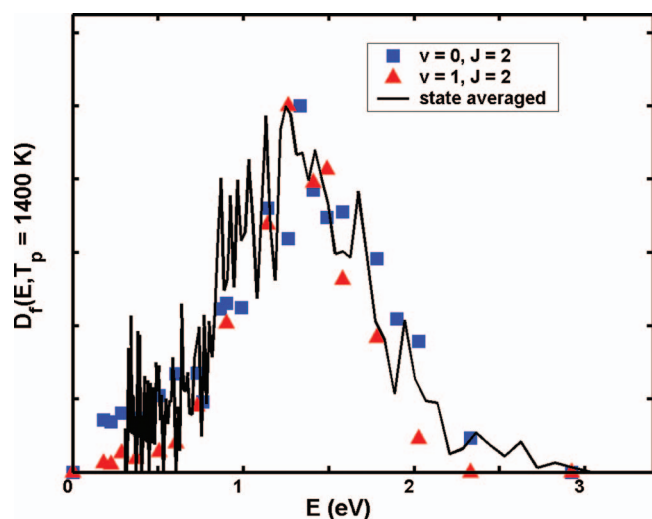

FIG. 3. $D_f(i, E, T_p)$ for D$_2$ (v=0, J=2) and D$_2$ (v=1, J=2) in arbitrary units as a function of normal translational energy E compared to that obtained previously in internal state averaged experiments (Ref. 11). All experiments are for Θ_D ~0.4 and for a T-jump to T_p ~1400 K. Relative intensities between each experiment are arbitrarily normalized to the same peak magnitude.
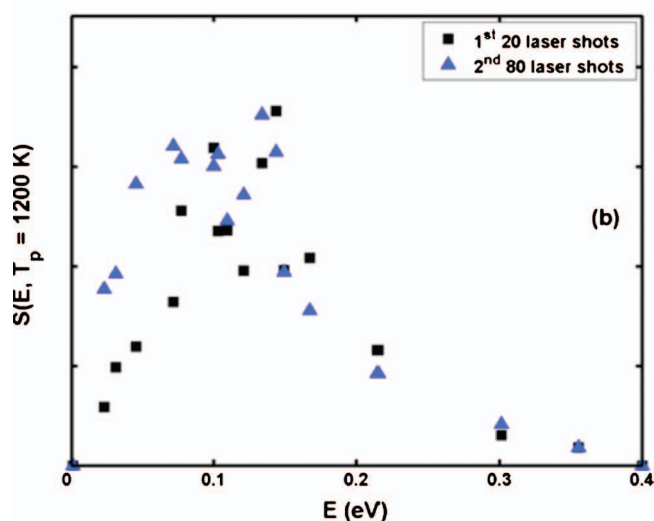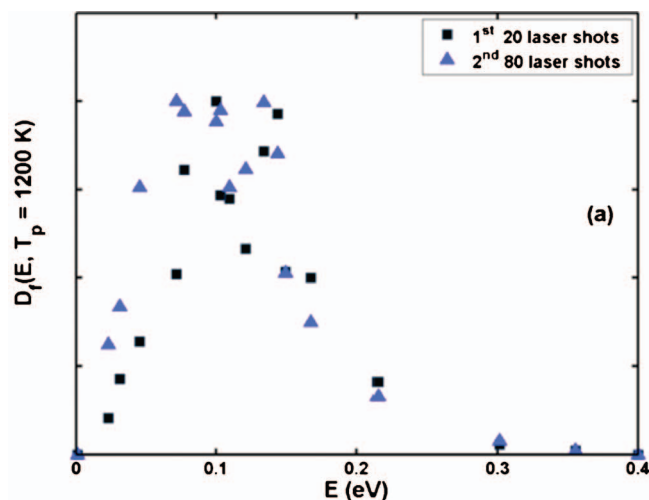

FIG. 4. (a) $D_f(E, T_p = 1200$ K) for D atoms desorbed from $\Theta_D \approx 0.4$ chemisorbed on C(0001) induced by repeated laser T-jumps to $T_p = 1200$ K in arbitrary units. Results averaged over first 20 laser shots are separated from those averaging over the second 80 laser shots. (b) $S(E, T_p = 1200$ K) (in arbitrary units) obtained from the results in (a) via detailed balance.

assisted associative desorption into the differentially pumped rotating mass spectrometer.[11] The latter has a TOF distance $l \approx 10$ cm in which there was little absolute error. The good agreement between the $D_f(i, E, T_s)$ for D$_2$ obtained with REMPI to the previous experiments demonstrates that l is accurately determined in the REMPI experiments. Note that the high E side of $D_f(i, E, T_s)$ is reduced by ~0.3 eV in v =1 relative to that of v=0. This appears to be slightly less than the D$_2$ vibrational frequency of 0.37 eV.

Because the D atom desorption seems to occur in two distinct groups during repeated laser shots due to the nearly biexponential bleaching dependence (see Figs. 1 and 2), the TOF spectra have been obtained separately for the two groups. The D atom TOF corresponding to R_i bleaching is obtained by averaging the TOF for the first 20 laser shots, while that following R_m bleaching is obtained by averaging the second 80 laser shots. Figure 4(a) shows $D_f(i, E, T_s)$ obtained from the D atom TOF for the two fractions following a T-jump to T_p ~1200 K and Fig. 4(b) shows these results converted to $S(i, E, T_s)$ via detailed balance. Note that the

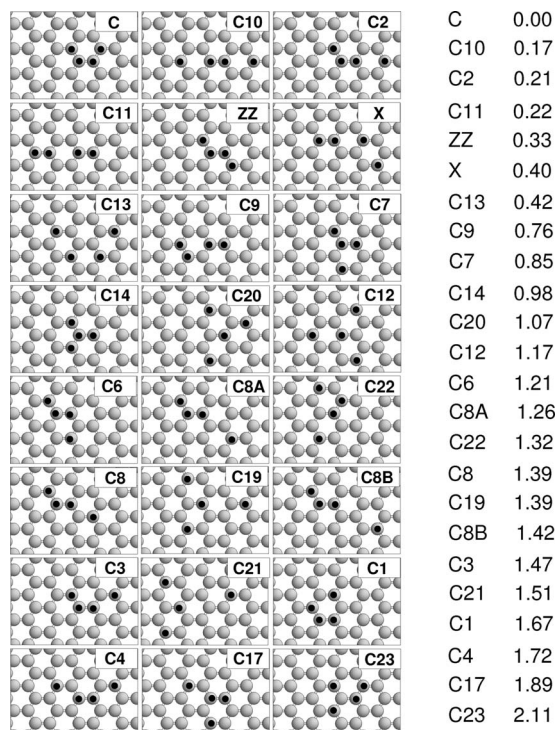|	
C	0.00
C10	0.17
C2	0.21
C11	0.22
ZZ	0.33
X	0.40
C13	0.42
C9	0.76
C7	0.85
C14	0.98
C20	1.07
C12	1.17
C6	1.21
C8A	1.26
C22	1.32
C8	1.39
C19	1.39
C8B	1.42
C3	1.47
C21	1.51
C1	1.67
C4	1.72
C17	1.89
C23	2.11

FIG. 5. Various 4H cluster configurations considered in the DFT calculations. The right hand side of the figure lists the energies of the clusters relative to the most stable one, ΔE_j, in ascending order. All energies are in eV.
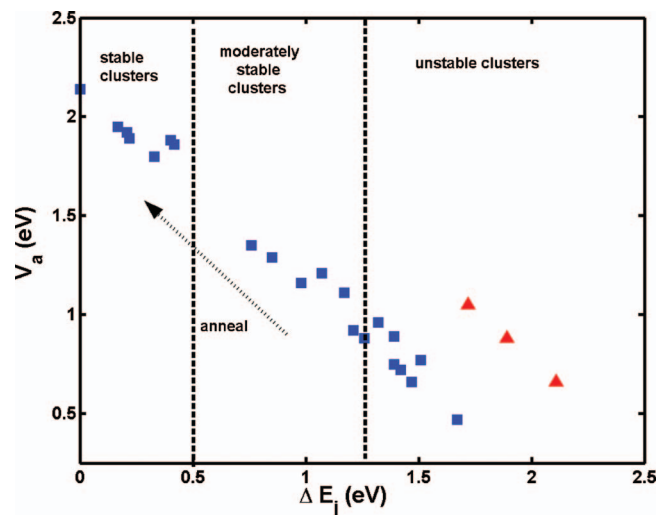

FIG. 6. Atomic desorption barriers V_a in eV from the various clusters in Fig. 5 vs the cluster energy relative to the most stable 4H cluster, ΔE_j in eV. The dotted lines denote the separation between the qualitative classes of clusters. The arrow labeled anneal shows the relative movement of clusters due to thermal annealing.

second fraction following R_m bleaching has a tail to a slightly lower E in $D_f(i,E,T_s)$ and consequently also in $S(i,E,T_s)$ relative to the initial fraction with R_i bleaching. The low signal/noise in this plot is due to a substantial variation in shot to shot D atom desorption flux due to UV laser intensity fluctuations, T-jump laser intensity fluctuations, variations in the laser irradiation spot, and in the D atom dosing. Random averaging the desorption at each t over each possible variable ensured that the true TOF was obtained without experimental artifact.

IV. DFT CALCULATIONS

The DFT calculations were performed with the plane wave based DACAPO program package,[20] applying ultrasoft pseudopotentials[21] to describe electron-ion interactions, and the Perdew–Wang functional (PW91) (Ref. [22]) for the electronic exchange correlation effects. The electron wave functions and augmented electron density were expanded in plane waves with cutoff energies of 25 and 140 Ry, respectively. The Chadi–Cohen scheme[23] with six special points was used for sampling of the surface Brillouin zone. The graphite surface was modeled with rhombohedral, periodically repeated slabs consisting of one graphite sheet with 72 carbon atoms, and separated by 15 Å of vacuum. The potential energy curves for diffusion of H atoms on graphite surfaces were calculated applying the nudged elastic band method.[24] Details of the DFT calculations will be presented elsewhere.[10]

Figure 5 shows a large variety of 4H (or 4D) atom clusters considered in the DFT. Also shown at the side of Fig. 5

are the DFT energies of the cluster configurations relative to the most stable cluster configuration ΔE_j, where j refers to the cluster label in Fig. 5. There is obviously a wide distribution of cluster stabilities, which for the purposes of later discussion we simply break into three classes: stable clusters ($\Delta E_j < 0.6$ eV), moderately stable clusters (0.6 eV $< \Delta E_j < 1.2$ eV), and unstable clusters ($\Delta E_j > 1.2$ eV). Calculations on 5H atom and 6H atom clusters also show a similar wide distribution of cluster stabilities and will be reported separately.[10] Therefore, we take the 4H clusters as qualitatively representative for all of the complex and possibly larger clusters present in C(0001) with large Θ_H. We also note that there should be no isotopic difference in any of the cluster energies, and only miniscule isotopic zero point energy differences for any of the barriers V_i describing the chemical processes. Therefore, theoretical chemical processes on D covered C(0001) are essentially identical to those from the DFT calculations on H covered C(0001) so that the H or D labels are used interchangeably.

The barriers to H atom desorption from the various clusters are estimated simply as the energy of the desorption process, $V_a \approx E_l(3H) + E_H(g) - E_j(4H)$, where $E_j(4H)$ is the energy of formation of the j four atom H cluster, $E_l(3H)$ is the energy of formation of the l three atom H cluster left on the surface by desorption of the least stably bound H atom and $E_H(g)$ is the energy of formation of the H atom in the gas phase. Direct DFT calculations of barriers to H atom addition V_H for 2H and 3H clusters suggest that desorption barriers estimated via this method are accurate for the stable clusters, but may underestimate the full barrier by <0.2 eV for the less stable clusters. Since these corrections are quite small relative to the variation of V_a with cluster configuration j, we do not attempt to correct V_a for the small barrier to H addition from the gas phase. A plot of the barriers V_a versus ΔE_j is given in Fig. 6 and clearly demonstrates an approximate inverse linear relationship between V_a and ΔE_j. The points given by the triangles correspond to the case where atomic
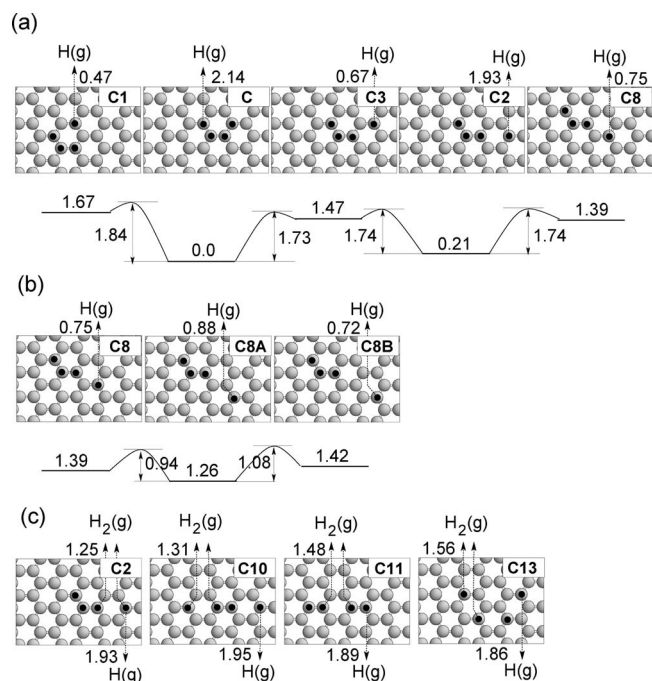
(a)

(b)

(c)

FIG. 7. (a) Pathways for thermal annealing and chemistry for some of the 4H clusters predicted by DFT that are induced by the laser T-jumps. All energies are in eV and calculated by DFT, i.e., cluster energies ΔE_j diffusion barriers and atomic desorption barriers. Diffusion barriers between different cluster configurations are shown directly while the atomic desorption barriers are simply given as labels on the arrows showing the desorbed atom. (b) Diffusion leading to disproportionation of a cluster and competing atomic desorption barriers. Notation is the same as in (a). (c) Associative desorption barriers (and atomic ones) for some of the low barrier associative desorption paths in the stable clusters. Notation is the same as in (a).

desorption leaves an unstable trimer on the surface. The qualitative classes of clusters are also marked on the figure.

Figure 7(a) shows some diffusion paths for transformation among some of the 4H clusters. Also indicated in Fig. 7(a) are some of the barriers to H atom desorption V_a from the clusters. Diffusion barriers V_d between cluster configurations j and k are either calculated directly in the DFT or estimated from the empirical relationship $V_d = 1.04$ eV $+ 0.5(\Delta E_k - \Delta E_j)$, which has previously been shown to give a good fit to the DFT calculated diffusion barriers.[25] Figure 7(b) shows diffusion barriers for the disproportionation of cluster C8, i.e., for an H atom to diffuse away from the cluster. Also indicated in Fig. 7(b) are the barriers for atomic desorption. Figure 7(c) shows barriers to associative desorption V_m from some of the stable clusters. These H₂ desorption barriers are calculated directly via DFT using the nudged elastic band method.[24]

V. DISCUSSION

While the cluster configurations considered in Fig. 5 are not exhaustive, it is apparent that most of the stable clusters contain predominately ortho-H configurations. Stable 5H and 6H clusters also show a preponderance of ortho-H configurations. This observation is in good agreement with angle resolved x-ray absorption experiments which demonstrate that the ortho configuration dominates at high Θ_H on C(0001).[9]

The D dosing and all subsequent T-jump experiments have been performed at a resting surface temperature T_s = 290 K. There may be some initial preferential formation of more stable clusters at very low Θ_D due to the lower barrier to D atom adsorption in these clusters,[8] but extended exposure to the D beam should produce nearly all possible clusters and cluster configurations. While careful monitoring of the time scale during the experiments was not recorded, T-jump experiments were not initiated until typically 10 min after H exposure by the atom source and continued for typically 5 min longer. Assuming normal pre-exponential factors ($\sim 10^{13}$ s^{-1}) for all kinetics (diffusion, atom desorption), this time scale implies that all cluster structures with barriers V_i ≤ 0.9 eV will not be probed during the subsequent T-jump experiments. From Fig. 6, this means that most if not all of the unstable clusters will no longer exist during the T-jump experiments since they will have already transformed into more stable structures on C(0001) by D atom diffusion or atomic desorption. During typical T-jump experiments, the surface transiently reaches $T_p \geqslant 300$ K, causing both desorption of D and D₂, as well as extensive annealing via D atom diffusion of the remaining cluster structures to the most stable cluster configurations. As Fig. 6 demonstrates, V_a is inversely related to the stability of the clusters configurations. Thus, the moderately stable cluster configurations exhibit the fastest atomic desorption rate and therefore dominate the initial R_i fraction. As the moderately stable clusters anneal by repeated T-jumps, only atomic desorption from the most stable clusters is possible and it is these which dominate atomic desorption described by the R_m fraction. Figure 7(a) illustrates the competition between thermal annealing of unstable clusters by diffusion with atomic desorption in the DFT calculations. Annealing generally wins in TPD because of the lower barriers to diffusion relative to atomic desorption from these clusters However, for the fast T-jump to very high temperatures, both processes are substantial.

Figure 7(b) indicates that it is unlikely for unstably bound atoms to diffuse away from the unstable clusters, i.e., for the clusters to disproportionate. H atom desorption barriers along the disproportionation path are generally less than diffusion barriers so that the atom generally desorbs before it can escape via diffusion.

For atomic desorption, $D_f(i,E,T_p)$ is converted to $S(i,E,T_p)$ via detailed balance, Eq. (2), in order to compare with dynamical calculations of atom sticking on C(0001).[13] Figure 4 separates the two desorbing fractions, i.e., those following R_i bleaching (moderately stable clusters) and those following R_m bleaching (stable clusters). For both groups, there is an initial increase in S with E followed by a decrease at higher E. The initial increase with E is most pronounced for the moderately stable clusters (R_i bleaching) since S for the stable clusters (R_i bleaching) tails to lower E. This implies that the stable clusters have slightly lower barriers to atomic adsorption than moderately stable ones. This has previously been observed in DFT calculations for 2 and 3 atom clusters.[8,13]

Kerwin and Jackson performed state of the art "first principles" calculations of the sticking of H (D) on C(0001) based on classical dynamics on a DFT based PES.[13] This

PES includes direct coupling to lattice coordinates describing the puckering of the C out of the plane that is necessary for the H (D) to form a bond to the graphite. Dissipation of energy from the nascent energy rich C–H bond to the rest of the graphite lattice, a necessary condition for sticking, is included by coupling the local DFT PES to a large cluster of graphite atom lattice vibrations. On the bare surface, a threshold in S is observed at the atomic adsorption barrier V_H (or V_D) (0.24 in their calculations), followed by a steep increase in S peaking at ~0.5 eV and then a decrease. The decrease in S with E is due to the increasing difficulty in dissipating the excess energy in the nascent C–H(D) bond. When this excess energy is not fully dissipated within a few C–H(D) vibrational periods, the H(D) does not remain bound to the C(0001). Because barriers for sticking of additional H(D) to an already adsorbed H(D) are often smaller than the initial barrier for a single H(D) adsorption, Kerwin and Jackson have also shown via related model PES that as V_H decreases, the entire S peak shifts to lower E. We anticipate that addition of D to existing clusters will exhibit a range of low atomic adsorption barriers V_D and that sticking at higher Θ_D should be best approximated by an average of the S curves for several low V_D. Thus, the "first principles" S (Fig. 5 of Ref. 13) are qualitatively consistent with the experimental results in Fig. 4(b). It does appear, however, that the theoretical calculations slightly overestimate the stabilization of excess energy in the nascent C–D bond since the calculated S tails to higher E than is observed experimentally.

We also see in Fig. 1 that D_2 associative desorption occurs principally from the most stable cluster configurations. The associative desorption barriers V_m for most of the cluster configurations of Fig. 5 have not been calculated via DFT. However, the V_m for four low associative desorption paths are shown in Fig. 7(c) indicate that V_m for the *trans*-configurations in these clusters are quite close to the 1.4 eV barrier of the *trans*-dimer that dominates associative desorption at low Θ_D.[6] We certainly anticipate that local *trans*-configurations in the larger clusters will dominate associative desorption from these as well. All of these clusters are in the most stable category.

The translational energy normal to the surface E released in associative desorption at the surface temperature T_p is given as[11]

$$E = V_{D_2} + \langle E_{th} \rangle_{T_p} + \tfrac{1}{2}k_B T_p - E_{\parallel} - \varepsilon_i - \varepsilon_s, \qquad (3)$$

where V_{D_2} is the barrier to dissociation of D_2 from the gas phase to form a given cluster configuration, $\langle E_{th} \rangle_{T_p}$ is the thermal energy in the transition state in modes perpendicular to the reaction coordinate at surface temperature T_p, $(1/2)k_B T_p$ is the thermal energy along the reaction coordinate, $E_{\parallel}$ is the translational energy parallel to the surface, ε_i is the internal energy of state i of D_2, and ε_s is the energy loss to the C(0001) surface during associative desorption. Note that $E_{\parallel} \sim 0$ due to the peaking nearly normal to the surface in the angular distribution of $D_f(E, T_p)$.[11] The thermal energy at the transition state added to V_{D_2} is modest (<0.3 eV). As shown in Fig. 3 and discussed earlier, $D_f(E, T_p)$ summed over all internal states produced in asso-

ciative desorption is a very broad distribution in E peaking at ~1.3 eV. It was previously unclear whether the moderate average translational energy (relative to the anticipated total available energy of ~3.4 eV) and very broad distribution were due to a wide distribution of internal states produced in the associative desorption, a wide distribution of lower V_{D_2} from different clusters or due to a large ε_s and distribution in ε_s. The state resolved measurements in Fig. 3 clearly demonstrate that the distribution of internal states produced in associative desorption is not the dominant loss and broadening mechanism. The barriers to associative desorption for the four clusters in Fig. 7(c) combined with the binding energies for the dimers remaining on the surface gives $\langle V_{D_2}(\text{DFT}) \rangle \approx 2.5 \pm 0.35$. A similar $\langle V_{D_2}(\text{DFT}) \rangle$ is obtained for associative desorption from a wide range of *trans*-clusters with four, five, and six atoms assuming an associative desorption barrier of ~1.4 eV from all clusters. Thus, the observed $\langle E \rangle \ll \langle V_{D_2}(\text{DFT}) \rangle + \langle E_{th} \rangle_{T_p}$ and the breadth of the observed distribution in E are much greater than that predicted via DFT. The only significant term not included in this comparison is the energy loss to the surface, and this implies that the average energy lost to the surface, $\langle \varepsilon_s \rangle > 1$ eV and that there is a broad distribution of such energy losses. This is consistent with the fact that the lattice distortion energy is ~1 eV/H atom in the adsorbed state (for the dimers),[26] and much of this is undoubtedly retained in the surface during associative desorption. Thus the response of the lattice to the release of the puckering configuration in associative desorption seems midway between an adiabatic and sudden response.

As noted earlier, the shift in the high energy region of $D_f(v=0, J=2, E, T_p)$ relative to $D_f(v=1, J=2, E, T_p)$, $\Delta D_f = 0.3$ eV implies a large vibrational efficacy $\eta_v = \Delta D_f / \Delta \varepsilon_v = (0.3/0.37) \approx 0.8$. This is entirely consistent with the extended D_2 bond length in the transition state in the DFT calculations.[4,6]

VI. SUMMARY AND CONCLUSIONS

REMPI detection shows that D atoms desorb directly into the gas phase following a laser induced T-jump of D chemisorbed on C(0001) at various initial coverages Θ_D. Bleaching experiments with repeated laser T-jumps to peak temperature T_p suggest that there are qualitatively two different classes of clusters since the bleaching is roughly biexponential, i.e., less stable ones with weakly bound D (fast initial bleaching R_i) and more stable ones with more strongly bound D (slower bleaching R_m). TOF experiments measure the energy resolved desorption flux $D_f(i, E, T_p)$ which is converted to energy dependent atomic sticking $S(i, E, T_p)$ by detailed balance. These experiments show that the more stable clusters have slightly lower barriers to atomic adsorption than the less stable clusters, in agreement with DFT calculations. The atomic adsorption inferred from the experiments is in reasonable accord with first principles theoretical calculations of sticking.[13] In addition, state resolved D_2 associative desorption is observed by REMPI using TOF techniques. The state resolved translational energy distributions are similar to those observed previously with internal state averaging.[11] This result, when combined with DFT estimates

of the total energy released for the various clusters, implies that there is substantial energy loss to the surface in associative desorption and that the large broadening in the translational energy distributions is due to a wide distribution of energy losses to the surface. Shifts in the high energy threshold between v=0 and v=1 D$_2$ produced in the associative desorption suggest a high vibrational efficacy for the dissociative adsorption/associative desorption chemistry.

We report a variety of DFT calculations on 4H(D) clusters on C(0001) that not only support the qualitative interpretation of the experiments, but also provide much a more quantitative physical picture of the chemical processes induced by the T-jump. The calculations demonstrate that a wide variety of cluster stabilities ΔE_j exist, as well as a wide range of diffusion barriers V_d between the different cluster configurations and barriers to atomic desorption V_a. Barriers to associative desorption from clusters containing *trans*-configurations are similar to those for dimer desorption. These calculations suggest that thermal annealing is a complex combination of atomic desorption, atomic diffusion to more stable cluster configurations, and associative desorption. The clusters are arbitrarily divided into three classes: unstable, moderately stable, and stable to connect with the experimental discussion. The unstable clusters are probably not observed in the experiments since atomic desorption/ diffusion converts the clusters to moderately stable ones prior to the T-jump. The moderately stable clusters have the lowest V_a and are desorbed most easily (R_i fraction), while the most stable clusters have higher V_a and are more difficult to desorb (R_m fraction). V_d between two cluster configurations always favors formation of the more stable configuration, so that repeated T-jumps will always anneal the clusters to the most stable ones.

ACKNOWLEDGMENTS

[1] D. Hollenbach and E. E. Salpeter, Astrophys. J. **163**, 155 (1971).
[2] T. Henning and F. Salama, Science **282**, 2204 (1998); E. Rauls and L. Hornekaer, Astrophys. J. **679**, 531 (2008).
[3] L. Jeloaica and V. Sidis, Chem. Phys. Lett. **300**, 157 (1999).
[4] X. W. Sha and B. Jackson, Surf. Sci. **496**, 318 (2002).
[5] T. Zecho, A. Guttler, X. W. Sha, B. Jackson, and J. Kuppers, J. Chem. Phys. **117**, 8486 (2002).
[6] L. Hornekær, Z. Sljivancanin, W. Xu, R. Otero, E. Rauls, I. Stensgaard, E. Laegsgaard, B. Hammer, and F. Besenbacher, Phys. Rev. Lett. **96**, 156104 (2006).
[7] A. Guttler, T. Zecho, and J. Kuppers, Chem. Phys. Lett. **395**, 171 (2004).
[8] L. Hornekær, E. Rauls, W. Xu, Z. Sljivancanin, R. Otero, I. Stensgaard, E. Laegsgaard, B. Hammer, and F. Besenbacher, Phys. Rev. Lett. **97**, 186102 (2006).
[9] A. Nikitin, L. A. Naslund, Z. Y. Zhang, and A. Nilsson, Surf. Sci. **602**, 2575 (2008).
[10] Z. Sljivancanin and B. Hammer (to be published).
[11] S. Baouche, G. Gamborg, V. V. Petrunin, A. C. Luntz, A. Baurichter, and L. Hornekaer, J. Chem. Phys. **125**, 084712 (2006).
[12] T. Zecho (private communication).
[13] J. Kerwin and B. Jackson, J. Chem. Phys. **128**, 084702 (2008).
[14] J. Kerwin, X. W. Sha, and B. Jackson, J. Phys. Chem. B **110**, 18811 (2006).
[15] T. Zecho, A. Guttler, and J. Kuppers, Carbon **42**, 609 (2004).
[16] G. G. Andersen, M.S. thesis, University of Southern Denmark, 2006.
[17] L. Diekhöner, H. Mortensen, A. Baurichter, and A. C. Luntz, J. Chem. Phys. **115**, 3356 (2001).
[18] G. C. Bjorklund, C. P. Ausschnitt, R. R. Freeman, and R. H. Storz, Appl. Phys. Lett. **33**, 54 (1978).
[19] E. E. Marinero, C. T. Rettner, and R. N. Zare, Phys. Rev. Lett. **48**, 1323 (1982).
[20] B. Hammer, L. B. Hansen, and J. K. Norskov, Phys. Rev. B **59**, 7413 (1999); S. R. Bahn and K. W. Jacobsen, Comput. Sci. Eng. **4**, 56 (2002).
[21] D. Vanderbilt, Phys. Rev. B **41**, 7892 (1990); K. Laasonen, A. Pasquarello, R. Car, C. Lee, and D. Vanderbilt, *ibid.* **47**, 10142 (1993).
[22] J. P. Perdew, J. A. Chevary, S. H. Vosko, K. A. Jackson, M. R. Pederson, D. J. Singh, and C. Fiolhais, Phys. Rev. B **46**, 6671 (1992).
[23] D. J. Chadi and M. L. Cohen, Phys. Rev. B **8**, 5747 (1973).
[24] H. Jonsson, G. Mills, and K. W. Jacobsen, in *Classical and Quantum Dynamics in Condensed Phase Simulations*, edited by B. J. Berne, G. Cicotti, and D. F. Coker (World Scientific, Singapore, 1998).
[25] H. M. Cuppen and L. Hornekaer, J. Chem. Phys. **128**, 174707 (2008).
[26] Z. Sljivancanin, E. Rauls, L. Hornekaer, W. Xu, F. Besenbacher, and B. Hammer J. Chem. Phys. 131, 084706 (2009)..